Journal of Magnetic Resonance **140,** 242–249 (1999)
Article ID jmre.1999.1849, available online at http://www.idealibrary.com on IDEAL®

High-Order Spin Diffusion Mechanisms in ^{19}F 2-D NMR of Oxyfluorides

Lin-Shu Du,* Malcolm H. Levitt,† and Clare P. Grey*

** Department of Chemistry, SUNY Stony Brook, Stony Brook, New York 11794-3400, and † Physical Chemistry Division, Stockholm University, S-10691 Stockholm, Sweden*

Received April 21, 1999

Negative cross-peaks have been observed in the ^{19}F 2-D magnetization-exchange MAS NMR spectra of $Ba_2MoO_3F_4$ under fast-spinning conditions. The polarization transfer dynamics are studied as a function of the spinning frequency and the frequency separation of the resonances. The results are consistent with a novel mechanism, in which four spins simultaneously exchange Zeeman magnetization with each other, in an energy-conserving process.

Key Words: **spin diffusion; magnetization transfer; 2-D NMR; ^{19}F; inorganic fluorides.**

INTRODUCTION

A variety of oxyfluorides have been studied by ^{19}F MAS NMR in order to probe the fluoride-ion distributions (*1*). The chemical shift ranges for many inorganic fluorides are not well understood and few semi-empirical correlations exist to help predict chemical shifts in these materials. We have explored a number of 2-D methods for studying fluorine–fluorine proximity in order to facilitate spectral assignment. In particular, the 2-D magnetization-transfer experiment (*2–4*) is useful for studying the local environment of nuclei in crystalline and amorphous solids. In the absence of chemical exchange, the main mechanism for magnetization transfer is the so-called spin diffusion process (*5–9*), which relies on the through-space magnetic dipolar coupling between nearby nuclear spins. Since the through-space coupling has an inverse cubic dependence on the internuclear distance, the observation of spin diffusion may be an indicator of spatial proximity, at least when experiments are performed over relatively short time scales.

The interpretation of spin diffusion is, however, complicated by its sensitivity to the chemical shift frequency differences between the associated spins. This may be the case for ^{19}F sites in inorganic fluorides, which often have large chemical shift differences. In order to assess the utility of spin diffusion for ^{19}F spectral assignment, we studied the compound $Ba_2MoO_3F_4$, which has a large range of ^{19}F chemical shifts.

If two molecular sites have a large chemical shift frequency difference, one expects rapid exchange of magnetization only when the rotational resonance conditions are met, i.e., when $(\omega_i^{iso} - \omega_j^{iso}) = n\omega_r$, where ω_i^{iso} and ω_j^{iso} are the isotropic shift frequencies of the two crystallographic sites, n is a small integer, and ω_r is the spinning frequency (*10–14*). At these conditions, the energy difference associated with the frequency separation between resonances of the two nuclear sites is compensated by a coherent exchange of energy with the mechanical rotation. This has been called rotor-driven spin diffusion (*13*). In systems containing abundant heteronuclear spins, such as protons, the energy difference involved in the magnetization transfer may sometimes be recovered by the interaction with the abundant spin system. In the case of protons, this has been termed proton-driven spin diffusion (*7, 15*).

The total spin angular moment in the direction of the static magnetic field is a good constant of the motion in high magnetic fields in the absence of RF irradiation. This implies, in turn, an approximate conservation of the total longitudinal magnetization along the field direction. If the magnetization of one spin site decreases, the magnetization of its exchange partner increases. This fact is reflected in the positive sign of cross-peaks in 2-D magnetization-exchange spectra.

Spin diffusion processes are, therefore, expected to have the following characteristics: (i) small rate constants when there is a large chemical shift frequency difference and the rotational resonance conditions are not met, and (ii) positive cross-peaks in 2-D magnetization-exchange spectra.

The spectra shown below display features which contradict both of these expectations: (i) finite cross-peaks are encountered even well away from a rotational resonance condition, and (ii) in some cases the cross-peaks are negative. We suggest an explanation of these results, which incorporates a higher order spin diffusion process, involving the simultaneous involvement of four spins rather than two. Such higher order processes have been suggested before in various contexts (*16, 17*), but the experimental evidence has always been somewhat ambiguous. In the results shown below, the higher order process is revealed through a spectral signature which is difficult to explain any other way.

EXPERIMENTAL

NMR. ^{19}F MAS NMR spectra were obtained with CMX-360 (8.4 T) and CMX-200 (4.7 T) spectrometers at operating

1090-7807/99 $30.00

frequencies for ^{19}F of −338.75 and −188.19 MHz, respectively. ^{19}F chemical shifts are expressed in ppm relative to liquid $CFCl_3$. A Chemagnetics pencil probe with a reduced ^{19}F background signal was used. This probe is equipped with a high-speed MAS stator and with 3.2-mm rotors that are capable of reaching spinning frequencies of 24 kHz. Due to the small size of the rotors, only approximately 50 mg of sample was required. Typically, 1-D spectra were acquired with $\pi/2$ pulses of duration 2 μs and recycle delays of 10 s, the spectra requiring approximately 100–500 acquisitions.

Two-dimensional spin-diffusion experiments were performed with a standard 2-D magnetization-exchange pulse sequence (*2*):

$$\pi/2\text{–}t_1\text{–}\pi/2\text{–}\tau_m\text{–}\pi/2\text{–acquire}\ (t_2).$$

Spectra are acquired (in t_2), for successive time increments of the first time dimension (t_1). The magnetization is aligned with the static magnetic field during the mixing time of the 2-D sequence (τ_m, which was always set equal to an integral number of rotor periods). Spin diffusion during τ_m is detected as a cross-peak in the 2-D spectrum after successive Fourier transformation along t_1 and t_2. 2-D spectra were acquired with $\pi/2$ pulses of duration 2 μs and recycle delays of 10 s, the spectra requiring approximately 64–128 acquisitions per time period increment. Spectra were collected at spinning frequencies of 18 kHz, at a field strength of 8.4 T, and at 10 and 23 kHz at a field strength of 4.7 T with mixing time intervals τ_m of 1 to 1000 ms.

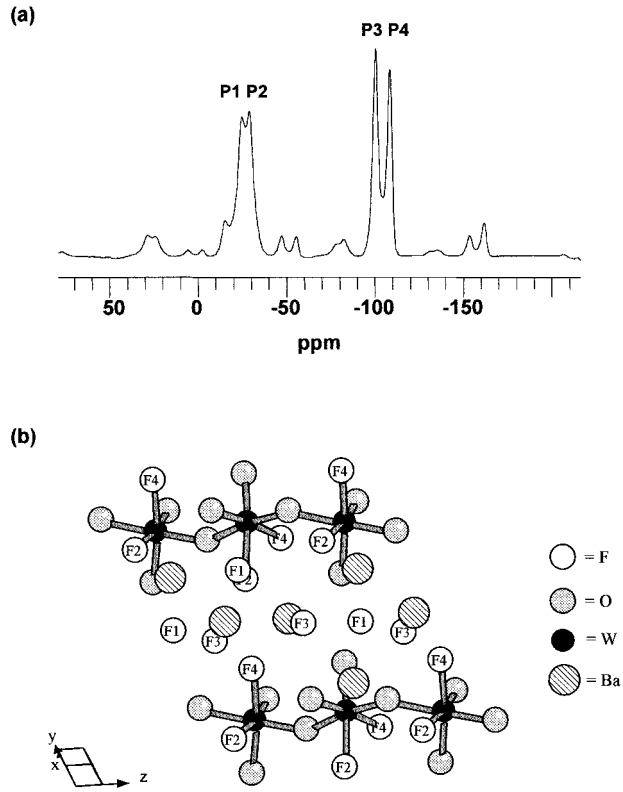

FIG. 1. (a) ^{19}F MAS NMR spectrum of $Ba_2MoO_3F_4$, collected at a spinning frequency of 18 kHz and a field strength of 8.4 T. (b) Crystal structure of the isostructural compound $Ba_2WO_3F_4$, showing the corner-shared WO_4F_2 octahedra, bridging oxygen atoms and proposed ordering of the cis oxygen and fluorine positions (*18*).

RESULTS

The ^{19}F MAS NMR spectrum of $Ba_2MoO_3F_4$ is shown in Fig. 1a. Two groups of resonances, P1/P2 and P3/P4, are observed at approximately −20 and −100 ppm, respectively, consistent with our earlier results (*1*). $Ba_2MoO_3F_4$ is isostructural with $Ba_2WO_3F_4$ (*18–20*), the structure of both these compounds consisting of chains of corner-sharing WO/F or MoO/F octahedra, separated by barium cations and two different anion sites (Fig. 1b). Oxygen ordering on three of the seven possible anion sites was proposed, by previous workers, to occur in $Ba_2WO_3F_4$ (*18–20*): One oxygen atom was located on the corner-sharing positions of the W–O/F octahedra (i.e., on the W–O–W chains), while the other two were located in a cis arrangement on the tungsten octahedra (Fig. 1b). We previously showed, by using ^{19}F MAS NMR, that the O/F ordering scheme in $Ba_2MoO_3F_4$ is similar to that proposed for $Ba_2WO_3F_4$, but that $Ba_2WO_3F_4$ contains considerable O/F disorder. Since the P1/P2 chemical shifts (Fig. 1a) in the spectrum of $Ba_2MoO_3F_4$ are close to the chemical shift of BaF_2 (−14.2 ppm), we assigned these resonances to fluoride ions located in between the Mo–O/F chains that are coordinated to four Ba atoms (labeled F1 and F3 in Fig. 1b (*18*)). The second group of resonances (P3 and P4) was then assigned to fluorine atoms coordinated to Mo atoms in the Mo chains (F2 and F4). This work has been described in detail elsewhere (*1*).

Figure 2a shows the 2-D spectrum of $Ba_2MoO_3F_4$, acquired with a mixing time interval of $\tau_m = 10$ ms at a field strength of 8.7 T (360 MHz for ^{1}H) and a spinning frequency of 18 kHz. This spinning frequency was chosen so as to avoid the rotational resonance conditions. The diagonal in the 2-D spectrum consists of the two groups of two resonances: P1/P2 and P3/P4. The cross-peaks between these resonances are seen more easily by taking horizontal slices through the peaks (e.g., P1 and P2, Fig. 2a): P1 is connected to a poorly resolved cross-peak from P2 (appearing as a shoulder of the diagonal peak) and also to a strong cross-peak from P3. In contrast, P2 is connected to a poorly resolved cross-peak from P1 and to a strong cross-peak from P4.

The 2-D spectra of $Ba_2MoO_3F_4$ at a field strength of 4.7 T with spinning frequencies of 10 and 23 kHz are shown in Figs. 2b and 2c. Both of these MAS frequencies are well away from any rotational resonance condition. The cross-peak intensities are much stronger at lower fields (Fig. 2b) than at higher fields (Fig. 2a). In addition, there are smaller differences in intensity between the P1–P3 and P1–P4 cross-peaks (and similarly for the P2–P3 and P2–P4 cross-peaks) at the lower field. Negative

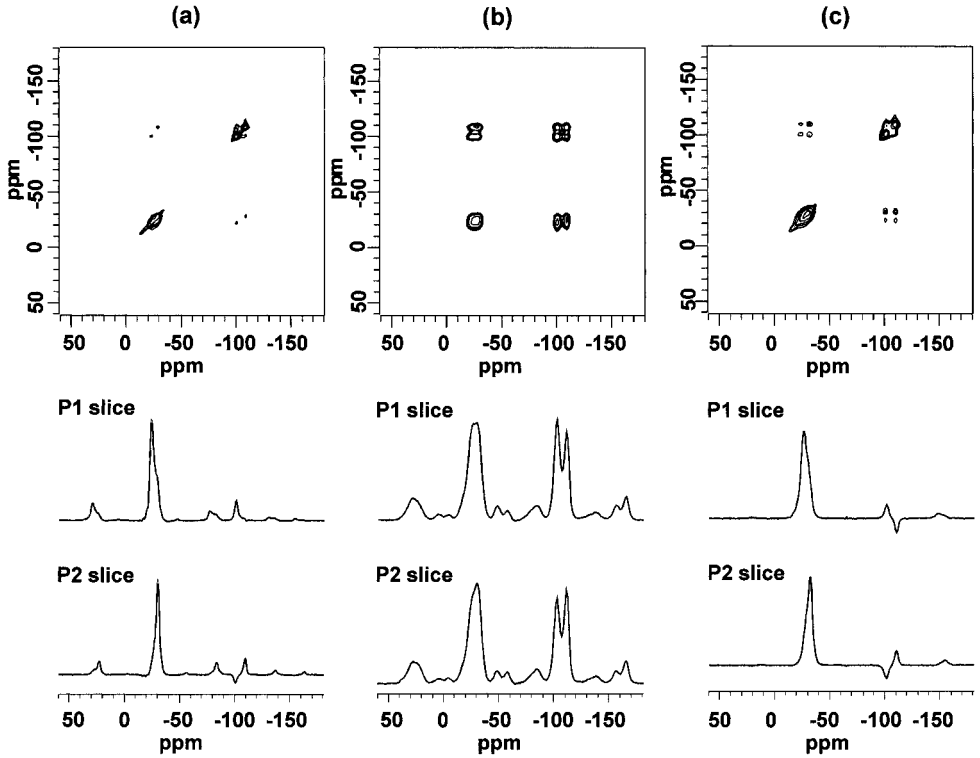

FIG. 2. (a) 2-D ^{19}F exchange spectrum of $Ba_2MoO_3F_4$ and slices parallel to the ω_2 axis at $\omega_1 = -24$ and -28 ppm (P1 and P2 slices, respectively), collected at a spinning frequency of 18 kHz with a mixing time of 10 ms at a field strength of 8.4 T. (b) and (c) 2-D ^{19}F exchange spectra of $Ba_2MoO_3F_4$ and its horizontal slices through P1 and P2, collected at a spinning frequency of 10 and 23 kHz, respectively, with a mixing time interval of 10 ms and a field strength of 4.7 T.

cross-peaks are observed at the lower field strength for P1–P4 and P2–P3 at a spinning frequency of 23 kHz (Fig. 2c). We repeated these 2-D experiments a number of times with slightly different experimental setups, in an attempt to exclude the possibility that these negative cross-peaks were due to an experimental artifact, but the spectra were always reproducible.

Figure 3 shows plots of the normalized and absolute cross-peak integrated intensities versus the mixing time interval for a spinning frequency of 23 kHz and a field strength of 4.7 T (the condition corresponding to Fig. 2c). These cross-peaks result from magnetization transfer from the P2 site. Each intensity plotted in Fig. 3a is normalized with respect to the total integrated amplitude of the 2-D spectral slice at the ω_1 coordinate of peak P2. At short mixing time intervals, P3 and P4 both grow in intensity as τ_m is increased, but in the negative sense for P3 and in the positive sense for P4. As τ_m is increased further, both cross-peaks decrease in intensity and the negative cross-peak eventually changes sign (at 700 ms). Figures 4a and 4b show plots of the normalized and absolute cross-peak integrated intensities versus the mixing time interval for a spinning frequency of 18 kHz and a field strength of 8.4 T (the condition corresponding to Fig. 2a). These cross-peaks result from magnetization transfer from the P2 site. An "up–down" spectral signature is also observed at short mixing time intervals. As τ_m is increased further, both cross-peaks decrease in intensity and the negative cross-peak eventually changes sign (at 70 ms).

DISCUSSION

In the usual spin-diffusion treatment for static solids, which derives from second-order perturbation theory (*21*), the rate constant for magnetization exchange between two sites i and j, W, is given by

$$W \approx \omega_D^2 F_{ij}(0), \qquad [1]$$

where ω_D is the dipolar coupling frequency,

$$\omega_D = -\left(\frac{\mu_0}{4\pi}\right)\left(\frac{\gamma^2\hbar}{r_{ij}^3}\right)\left(\frac{1}{2}\right)(3\cos^2\theta_{ij} - 1), \qquad [2]$$

which depends on the internuclear distance r_{ij} and on the angle θ_{ij} between the internuclear vector and the magnetic field. $F_{ij}(0)$ is the so-called overlap integral and it represents the zero-quantum spectral density at zero frequency. Effectively, it is a measure of the extent of overlap between the NMR resonances of the spins. The difference in chemical shifts between interacting spins affects the spin-diffusion rate via the

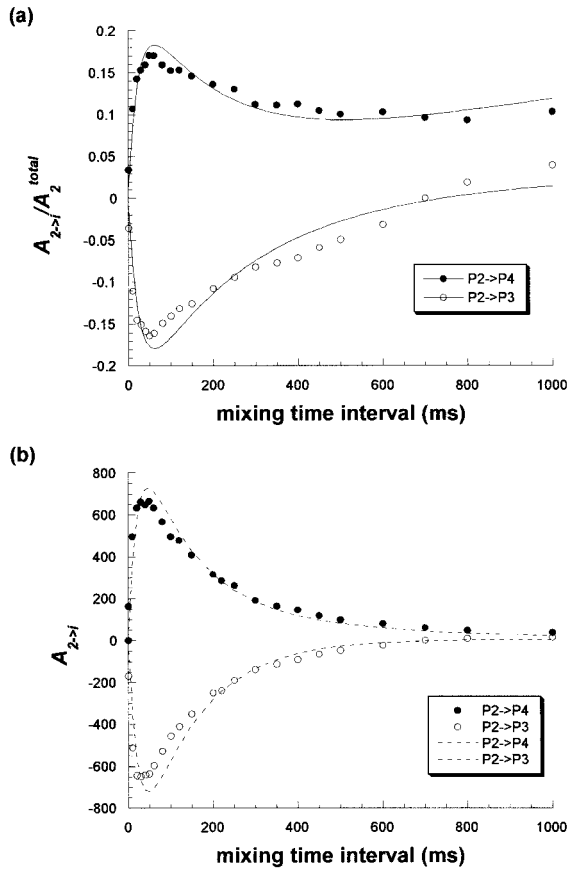

FIG. 3. Normalized cross-peak integrated intensities (circles) (a) and absolute cross-peak integrated intensities (arbitrary units) (b) versus the mixing interval. Data were extracted from horizontal slices of P2 (i.e., slices at the frequency $\omega_1 = -28$ ppm), taken from the 2-D spectra of $Ba_2MoO_3F_4$ collected with a spinning frequency of 23 kHz at a field strength of 4.7 T. The solid lines in (a) show the best fits obtained with Eqs. [26] and [27], while the dashed lines in (b) show simulations obtained by numerically diagonalizing Eq. [11] (see text). Values of 20/20, 2.1/1.9, and 0.16/0.02 s^{-1} for q, r, and s, respectively, were used in the simulations for P2 → P4/P2 → P3.

$F_{ij}(0)$ term. There are, thus, two main factors that dominate the magnetization-exchange process: the spatial distance and spectral frequency difference between the two nuclei. Since the magnetization-exchange rate is proportional to the square of the dipolar coupling strength, it is proportional to the inverse sixth power of the distance between the spins. Therefore, closer nuclei have an increased spin-exchange probability. However, spin diffusion may also be attenuated by a large chemical shift frequency difference, which leads to a reduction in the overlap integral $F_{ij}(0)$.

The equations must be modified in rotating solids, since the relevant perturbations become time-dependent. Nevertheless, an equivalent treatment may be used, if we allow the zero-quantum spectrum to split up into sidebands. Enhanced magnetization exchange is observed when a sideband of the zero-quantum spectrum is placed at zero frequency: These are the rotational resonances (*14*).

The results in Figs. 2a and 2b are reasonably consistent with this model, since decreasing the magnetic field decreases the chemical shift frequency separation and hence increases the overlap integral $F_{ij}(0)$. The cross-peaks are therefore more intense at lower magnetic fields.

The results shown in Fig. 2c are more unusual. These were obtained under fast-spinning conditions (23 kHz) and low magnetic field (4.7 T). The $n = 1$ rotational resonance would be observed at a spinning frequency of ~15 kHz at this field strength. This spectrum was therefore obtained at a spinning frequency much higher than that required for rotational resonance. One could anticipate cross-peaks of negligible amplitude in this case. Instead, all relevant slices of the 2-D spectrum contain significant cross-peaks, which form a characteristic up–down spectral pattern. The consistent appearance of negative cross-peaks is highly unusual and demands explanation.

Two facts are particularly relevant to an understanding of these cross-peaks: First, the difference between the P1 and P3

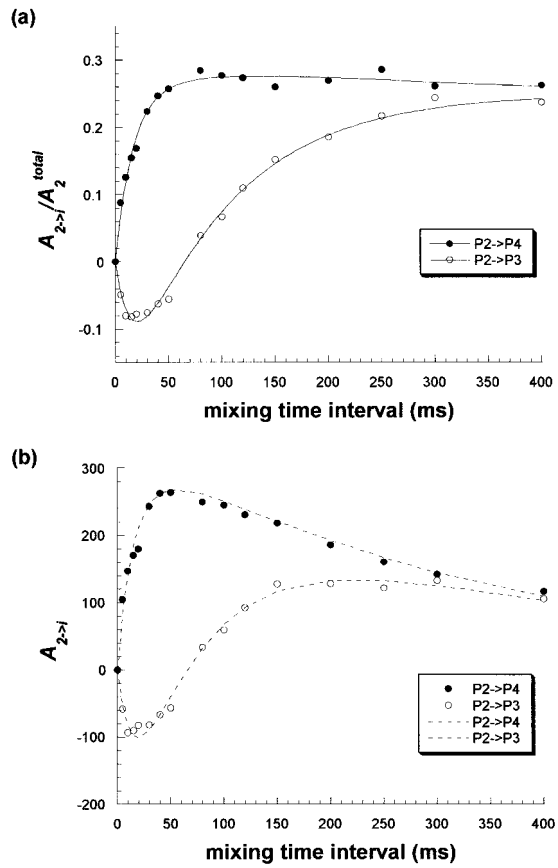

FIG. 4. Normalized cross-peak integrated intensities (circles) (a) and absolute cross-peak integrated intensities (arbitrary units) (b) versus the mixing interval from horizontal slices of P2 taken from the 2-D spectra of $Ba_2MoO_3F_4$ collected with a spinning frequency of 18 kHz at a field strength of 8.4 T. The solid lines in (a) show the best fits obtained with Eqs. [26] and [27], while the dashed lines in (b) show simulations obtained by numerically diagonalizing Eq. [11] (see text). Values of 28/28, 1.1/2.6, and 2.2/2.6 s^{-1} for q, r, and s, respectively, were used in the simulations for P2 → P4/P2 → P3.

chemical shifts is similar to that between P2 and P4 (76 and 80 ppm, respectively). Second, the distances between all four fluorine sites are similar (2.6–3.0 Å).

We now develop a kinetic model of a high-order spin-diffusion process, which is reasonably consistent with the experimental data.

Consider a system of four coupled spin-1/2, with resonances ω_1^0, ω_2^0, ω_3^0, and ω_4^0, arranged in two groups, such that

$$\omega_1^0 - \omega_3^0 \approx \omega_2^0 - \omega_4^0 \gg \omega_1^0 - \omega_2^0 \approx \omega_3^0 - \omega_4^0. \qquad [3]$$

Let us postulate a high-order magnetization-exchange process, which preserves the total Zeeman energy of the system. This is a prerequisite of any reasonably efficient magnetization-exchange process in the absence of an RF field. Since the Zeeman energy associated with a particular site is proportional to its resonance frequency, the conservation of Zeeman energy imposes a constraint on the system:

$$a_1\omega_1^0 + a_2\omega_2^0 + a_3\omega_3^0 + a_4\omega_4^0 = \text{constant}, \qquad [4]$$

where $a_i(t)$ is the longitudinal magnetization of spin i. Equation [4] can be rewritten, making use of Eq. [3] (i.e., $\omega_1^0 - \omega_3^0 \approx \omega_2^0 - \omega_4^0$ and $\omega_1^0 - \omega_2^0 \approx \omega_3^0 - \omega_4^0$), as

$$\frac{\partial}{\partial t}(a_1 + a_2 - a_3 - a_4) = 0. \qquad [5]$$

In addition, the spin Hamiltonian in a high magnetic field commutes with the total angular momentum operator along the field direction. This implies that any magnetization-exchange process must also conserve the total Zeeman angular momentum, and hence

$$\frac{\partial}{\partial t}(a_1 + a_2 + a_3 + a_4) = 0. \qquad [6]$$

It is convenient to define the terms

$$\Sigma_{12} \equiv a_1 + a_2;\ \Delta_{12} \equiv a_1 - a_2$$
$$\Sigma_{34} \equiv a_3 + a_4;\ \Delta_{34} \equiv a_3 - a_4. \qquad [7]$$

The above constraints then imply that

$$\frac{\partial}{\partial t}\sum_{12} \equiv \frac{\partial}{\partial t}(a_1 + a_2) = 0, \qquad [8]$$

and

$$\frac{\partial}{\partial t}\Sigma_{34} \equiv \frac{\partial}{\partial t}(a_3 + a_4) = 0. \qquad [9]$$

The equation of motion of the quantities Σ_{12}, Σ_{34}, Δ_{12}, and Δ_{34}, for the high-order spin-diffusion process may therefore be written

$$\frac{\partial}{\partial t}\begin{pmatrix}\Sigma_{12}\\ \Sigma_{34}\\ \Delta_{12}\\ \Delta_{34}\end{pmatrix} = \begin{pmatrix}0 & 0 & 0 & 0\\ 0 & 0 & 0 & 0\\ 0 & 0 & -q & q\\ 0 & 0 & q & -q\end{pmatrix} \cdot \begin{pmatrix}\Sigma_{12}\\ \Sigma_{34}\\ \Delta_{12}\\ \Delta_{34}\end{pmatrix}, \qquad [10]$$

where the symbol q represents the rate constant for the postulated high-order spin-diffusion process that corresponds to approximately energy-conserving transitions between states such as $|\alpha\beta\beta\alpha>$ to $|\beta\alpha\alpha\beta>$. Small energy balances may be absorbed by the dipolar reservoir. Equation [10] is consistent with a physical picture for this process where the difference polarizations Δ_{12} and Δ_{34} are in exchange: $\Delta_{12} \underset{q}{\overset{q}{\rightleftharpoons}} \Delta_{34}$, where q is the rate constant of this process. Such transitions have zero probability within the second-order level of perturbation theory, but may have finite probabilities at higher perturbation orders. In this paper, we do not attempt a theory of such processes, but merely examine their spectral consequences.

In order to describe the full kinetics of the system, Eq. [10] must be incorporated into a system of equations which also includes conventional relaxation and spin-exchange processes. The full equation of motion, in the basis set (Σ_{12}, Σ_{34}, Δ_{12}, Δ_{34}), can be described as

$$\frac{\partial}{\partial t}\begin{pmatrix}\Sigma_{12}\\ \Sigma_{34}\\ \Delta_{12}\\ \Delta_{34}\end{pmatrix} = \mathbf{K} \cdot \begin{pmatrix}\Sigma_{12}\\ \Sigma_{34}\\ \Delta_{12}\\ \Delta_{34}\end{pmatrix}, \qquad [11]$$

where the 4×4 matrix $\mathbf{K}$ is the complete kinetic matrix, which may be expressed as the combination of the 1-spin, 2-spin, and 4-spin kinetic matrices, i.e.,

$$\mathbf{K} = \mathbf{K}^{\text{1-spin}} + \mathbf{K}^{\text{2-spin}} + \mathbf{K}^{\text{4-spin}}. \qquad [12]$$

$\mathbf{K}^{\text{1-spin}}$ corresponds to the spin–lattice relaxation of the spin system and is given in the basis set (a_1, a_2, a_3, a_4) by

$$\mathbf{K}^{\text{1-spin}}_{(a_1,a_2,a_3,a_4)} = \begin{pmatrix} -R_1 & 0 & 0 & 0 \\ 0 & -R_2 & 0 & 0 \\ 0 & 0 & -R_3 & 0 \\ 0 & 0 & 0 & -R_4 \end{pmatrix}, \qquad [13]$$

where R_i (i = 1–4) is the spin–lattice relaxation rate constant of spin i. The thermal equilibrium term has been omitted from this equation, since phase cycling is used in the experiment, and this removes signals which derive from thermally equilibrated spin magnetization. The transformation matrix, **T**, given by

$$\mathbf{T} = \begin{pmatrix} 1 & 0 & 1 & 0 \\ 1 & 0 & -1 & 0 \\ 0 & 1 & 0 & 1 \\ 0 & 1 & 0 & -1 \end{pmatrix}, \qquad [14]$$

transforms the (Σ_{12}, Σ_{34}, Δ_{12}, Δ_{34}) basis set to the (a_1, a_2, a_3, a_4) basis set:

$$\begin{pmatrix} a_1 \\ a_2 \\ a_3 \\ a_4 \end{pmatrix} = \begin{pmatrix} 1 & 0 & 1 & 0 \\ 1 & 0 & -1 & 0 \\ 0 & 1 & 0 & 1 \\ 0 & 1 & 0 & -1 \end{pmatrix} \cdot \begin{pmatrix} \Sigma_{12} \\ \Sigma_{34} \\ \Delta_{12} \\ \Delta_{34} \end{pmatrix}. \qquad [15]$$

The 1-spin kinetic matrix, in the (Σ_{12}, Σ_{34}, Δ_{12}, Δ_{34}) basis, is therefore

$$\mathbf{K}^{\text{1-spin}} = \mathbf{T}^{-1} \cdot \begin{pmatrix} -R_1 & 0 & 0 & 0 \\ 0 & -R_2 & 0 & 0 \\ 0 & 0 & -R_3 & 0 \\ 0 & 0 & 0 & -R_4 \end{pmatrix} \cdot \mathbf{T}. \qquad [16]$$

$\mathbf{K}^{\text{2-spin}}$ represents the normal spin diffusion kinetic matrix,

$$\mathbf{K}^{\text{2-spin}} = \mathbf{T}^{-1} \cdot \begin{pmatrix} -(r_{12}+r_{13}+r_{14}) & r_{12} & r_{13} & r_{14} \\ r_{12} & -(r_{12}+r_{23}+r_{24}) & r_{23} & r_{24} \\ r_{13} & r_{23} & -(r_{13}+r_{23}+r_{34}) & r_{34} \\ r_{14} & r_{24} & r_{34} & -(r_{14}+r_{24}+r_{34}) \end{pmatrix} \cdot \mathbf{T}, \qquad [17]$$

where r_{ij} represents the "conventional" spin-diffusion rate constants for exchange of magnetization between sites i and j.

The 4-spin term of the high-order spin diffusion process has been described above and the equation of motion with the basis set (Σ_{12}, Σ_{34}, Δ_{12}, Δ_{34}) was already given in Eq. [10]. Thus, the 4-spin kinetic matrix may be written as

$$\mathbf{K}^{\text{4-spin}} = \begin{pmatrix} 0 & 0 & 0 & 0 \\ 0 & 0 & 0 & 0 \\ 0 & 0 & -q & q \\ 0 & 0 & q & -q \end{pmatrix}. \qquad [18]$$

The trajectory of the individual magnetization components (a_1, a_2, a_3, a_4) may be predicted by diagonalizing Eq. [12].

In the following discussion, we assume that the rate constant for magnetization exchange between sites 1 and 2 is similar to that for magnetization exchange between sites 3 and 4, i.e.,

$$r_{12} \approx r_{34} \equiv r. \qquad [19]$$

The rate constants for magnetization exchange between the two groups of resonances are also assumed to be similar, i.e.,

$$r_{13} \approx r_{14} \approx r_{23} \approx r_{24} \equiv s. \qquad [20]$$

In order to obtain an analytical solution to the equation of motion, we further assume that the relaxation rate constant for each spin is similar, i.e.,

$$R_1 \approx R_2 \approx R_3 \approx R_4 \equiv R. \qquad [21]$$

The relaxation rates were measured at a spinning frequency of 23 kHz and a field strength of 4.7 T, to check the validity of this assumption. Very similar relaxation rate constants, R_1, R_2, R_3, and R_4 of 3.20, 3.22, 3.35, and 3.50 s^{-1}, respectively, were obtained, suggesting that the errors associated with this assumption are small.

Consider now a slice of the 2-D spectrum parallel to the ω_2 axis and at $\omega_1 = \omega_1^0$. The trajectory of the spins 3 and 4 cross-peaks with respect to τ_m may be derived as

$$A_{1\to3}(t) = \tfrac{1}{4}\, a_1(0)(1 - e^{-4st} + e^{-2(r+s)t} - e^{-2(q+r+s)t})e^{-Rt}, \qquad [22]$$

$$A_{1\to4}(t) = \tfrac{1}{4}\, a_1(0)(1 - e^{-4st} - e^{-2(r+s)t} + e^{-2(q+r+s)t})e^{-Rt}. \qquad [23]$$

Similar expressions may be obtained for spectral slices through resonances ω_2, ω_3, and ω_4.

The ratio of the area of a cross-peak to the total intensity in a 2-D slice parallel to the ω_2 axis and at $\omega_1 = \omega_1^0$ can be expressed as

$$\frac{A_{1\to3}(t)}{A_1^{\text{total}}(t)} = \tfrac{1}{4}\,(1 - e^{-4st} + e^{-2(r+s)t} - e^{-2(q+r+s)t}), \quad [24]$$

$$\frac{A_{1\to4}(t)}{A_1^{\text{total}}(t)} = \tfrac{1}{4}\,(1 - e^{-4st} - e^{-2(r+s)t} + e^{-2(q+r+s)t}), \quad [25]$$

where $A_{i\to j}(t)$ is the integrated area under the cross-peak centered at coordinate $(\omega_1, \omega_2) = (\omega_i^0, \omega_j^0)$, and $A_i^{\text{total}}(t)$ is the total peak area of the slice parallel to the ω_2 axis and at $\omega_1 = \omega_1^0$ at mixing time interval $\tau_m = t$. Similar results can also be derived for the slices parallel to the ω_2 axis and at $\omega_1 = \omega_2^0$:

$$\frac{A_{2\to3}(t)}{A_2^{\text{total}}(t)} = \tfrac{1}{4}\,(1 - e^{-4st} - e^{-2(r+s)t} + e^{-2(q+r+s)t}), \quad [26]$$

$$\frac{A_{2\to4}(t)}{A_2^{\text{total}}(t)} = \tfrac{1}{4}\,(1 - e^{-4st} + e^{-2(r+s)t} - e^{-2(q+r+s)t}), \quad [27]$$

If the spin diffusion rates between the two groups of resonances are ignored ($s = 0$), Eqs. [26] and [27] can be further simplified:

$$\frac{A_{2\to3}(t)}{A_2^{\text{total}}(t)} = -\tfrac{1}{4}\,(e^{-2rt} - e^{-2(r+q)t}), \quad [28]$$

$$\frac{A_{2\to4}(t)}{A_2^{\text{total}}(t)} = \tfrac{1}{4}\,(e^{-2rt} - e^{-2(r+q)t}). \quad [29]$$

Note that these formulas predict an up–down spectral signature, which is qualitatively consistent with the experimental results in Fig. 2c.

Figure 3a shows the experimental intensity ratios of the cross-peaks connecting P2 and P3 and P2 and P4 versus mixing time interval τ_m, obtained from spectral slices at the frequency $\omega_1 = \omega_2^0$. The experimental normalized cross-peak amplitudes were simulated with Eqs. [26] and [27] (see solid lines in Fig. 3a). The 4-spin spin-diffusion rate constants obtained from these simulations ($q = 20 \pm 2$ and $20 \pm 2\ s^{-1}$, for P2 → P3 and P2 → P4, respectively) are higher than the spin-diffusion rate constants involving the spin exchange within the group ($r = 1.9 \pm 0.2$ and $2.1 \pm 0.2\ s^{-1}$, for P2 → P3 and P2 → P4, respectively) and are considerably larger than the spin-diffusion rate constants between the groups ($s = 0.02 \pm 0.02\ s^{-1}$ and $0.16 \pm 0.02\ s^{-1}$, for P2 → P3 and P2 → P4, respectively).

Although there is qualitative agreement between experiment and simulation, some discrepancies remain, which may have a number of causes. First, we have assumed that the relaxation time constants of all four groups are the same. Second, the cross-peak intensities were measured from the isotropic resonance only. In practice, there may be significant differences in the ratios of the intensities of the sideband to isotropic resonances between the different resonances. Third, the frequency separations between the two resonances within the two groups are not identical in the experimental system. The associated energy mismatch may prevent the high-order spin diffusion from proceeding to completion.

In order to explore whether any of the assumptions made in deriving the analytical solution to Eq. [11] are responsible for any of the observed differences between the experimental data and the simulations, the time evolutions of the absolute intensities of cross-peaks in the slices at the frequency $\omega_1 = \omega_2^0$ were obtained by numerically diagonalizing the matrix defined in Eq. [11]. Since no experimental data were available for a zero mixing interval, the amplitude $A_2^{\text{total}}(\tau_m = 0)$ was estimated from the measured value of A_2^{total} at $\tau_m = 1$ ms (4761 arbitrary units) using the equation $A_2^{\text{total}}(\tau) = A_2^{\text{total}}(0)e^{-R_2 t}$ and $R_2 = 3.22\ s^{-1}$. The estimate gave the value of $A_2^{\text{total}}(0) = 4776$ arbitrary units. The measured relaxation rate constants (R_1, R_2, R_3, and R_4) and the estimated values of q, r, and s were input into the matrix **K** which was then diagonalized. Values of q, r_{12}, r_{34}, r_{13}, r_{14}, r_{23}, and r_{24} (see Eq. [17]) were varied to obtain the closest match between the simulated and experimental data. The result of the absolute intensities of P2 → P3 and P2 → P4 versus the mixing interval and their curve-fittings are shown in Fig. 3b. The best fit using the experimental spin–lattice relaxation rates and numerical diagonalization gave very similar results to those obtained with the approximate analytical solutions. Further, no significant changes to the quality of the fit were obtained when the six coefficients r_{ij} were used instead of the two coefficients r and s. We, therefore, conclude that the assumptions underlying the analytical formulas are reasonable.

We have also studied the cross-peak behavior at a field strength of 8.4 T and a spinning frequency of 18 kHz, again chosen to avoid the rotational resonances. Negative cross-peaks were again observed at short mixing intervals ($\tau_m \approx 25$ ms). A fit to the high-field data, using Eqs. [26] and [27], is shown in Fig. 4a. Four-spin spin-diffusion rate constants (q) of 28 ± 3 and $28 \pm 3\ s^{-1}$, were obtained by fitting the P2 → P3 and P2 → P4 cross-peaks, respectively. These values are slightly larger than those obtained at the lower field (20 ± 2 and $20 \pm 2\ s^{-1}$, for P2 → P3 and P2 → P4, respectively). The rate constants extracted for spin diffusion within the group are similar to those obtained at the lower field: $r = 2.6 \pm 0.3$ and $1.1 \pm 0.3\ s^{-1}$, for P2 → P3 and P2 → P4, respectively, while those for spin diffusion between the two groups are much larger at the higher field: $s = 2.6 \pm 0.3$ and $2 \pm 1\ s^{-1}$, for P2 → P3 and P2 → P4, respectively.

The significant increase in the rate constants for 2-spin spin diffusion is presumably a consequence of the reduced spinning frequency of 18 kHz. Presumably, the slower spinning frequency results in a larger spectral overlap integral, in comparison to that at 4.7 T at a spinning speed of 23 kHz. The slight increase in the 4-spin spin-diffusion rate constant may also be due to the slower spinning frequency.

The time evolution of the absolute intensities of cross-peaks and their curve-fitting results are shown in Fig. 4b. The relaxation rate constants R_1, R_2, R_3, and R_4 (of 2.75, 2.78, 2.35, and 2.44 s^{-1}, respectively, at a spinning speed of 18 kHz and a field strength of 8.4 T), obtained from the T_1 measurements, were input in the matrix **K** in Eq. [11] along with estimated values of q, r_{12}, r_{34}, r_{13}, r_{14}, r_{23}, and r_{24}, and the matrix was diagonalized numerically. A value for $A_2^{\text{total}}(0)$ of 1183 arbitrary units was determined in a separate experiment. Again the simulations are very similar to those obtained with the analytical expression (Fig. 4a), and almost identical values of q, r, and s were extracted.

These results show that it may not always be straightforward to use 2-D magnetization-exchange spectra to extract information concerning proximity between coupled spins. Many factors, such as frequency separations between resonances, are important, particularly at high spinning frequencies. If normal 2-spin spin diffusion is suppressed, high-order spin-diffusion processes may become significant. For the purpose of assignment, it may be better to employ RF recoupling schemes in the mixing interval of the 2-D experiment (*22–26*).

CONCLUSION

We have observed unusual negative cross-peaks in ^{19}F MAS 2-D spectra of inorganic fluorides. These cross-peaks could be rationalized by hypothesizing a high-order spin-diffusion process in which four spins participate simultaneously. A simple kinetic model for these cross-peaks is proposed, and qualitative fits with the experimental results are obtained. These results demonstrate that 2-D magnetization-exchange spectra in systems with large chemical shift differences and moderate dipolar couplings may be complicated by high-order magnetization-transfer processes. These processes may be important in any system that contains strongly coupled groups of spins with large chemical shift differences. Finally, the effect of large chemical shift differences in reducing the efficiency of magnetization transfer is expected to become increasingly important at higher fields.

ACKNOWLEDGMENTS

This research was supported by the National Science Foundation through the NYI program (DMR-9458017) and through a grant to purchase the NMR spectrometer (CHE-9405436). Helpful discussions with Dr. Z. Gan are gratefully acknowledged.

REFERENCES

1. L.-S. Du, F. Wang, and C. P. Grey, High-resolution ^{19}F MAS and ^{19}F-^{113}Cd REDOR NMR study of oxygen/fluorine ordering in oxyfluorides, *J. Solid St. Chem.* **140,** 285–294 (1998).
2. J. Jeener, B. H. Meier, P. Bachmann, and R. R. Ernst, Investigation of exchange processes by two-dimensional NMR spectroscopy, *J. Chem. Phys.* **71,** 4546–4553 (1979).
3. B. H. Meier and R. R. Ernst, Elucidation of chemical exchange networks by two-dimensional NMR spectroscopy: The heptamethylbenzenonium ion, *J. Am. Chem. Soc.* **101,** 6441–6442 (1979).
4. R. R. Ernst, G. Bodenhausen, and A. Wokaun, "Principles of Nuclear Magnetic Resonance in One and Two Dimensions," Clarendon Press, Oxford (1987).
5. N. Bloembergen, On the interaction of nuclear spins in a crystalline lattice, *Physica* **15,** 386–426 (1949).
6. C. E. Bronniman, N. M. Szeverenyi, and G. E. Maciel, ^{13}C spin diffusion of adamantane, *J. Chem. Phys.* **79,** 3694–3700 (1983).
7. D. Suter and R. R. Ernst, Spin diffusion in resolved solid-state NMR spectra, *Phys. Rev. B* **32,** 5608–5627 (1985).
8. D. L. Vanderhart, Natural-abundance ^{13}C–^{13}C spin exchange in rigid crystalline organic solids, *J. Magn. Reson.* **72,** 13–47 (1987).
9. B. H. Meier, Polarization transfer and spin diffusion in solid-state NMR, in "Advances in Magnetic and Optical Resonance" (W. S. Warren, Ed.) Vol. 18, pp. 1–116, Academic Press, San Diego (1994).
10. E. R. Andrew, A. Bradbury, R. G. Eades, and V. T. Wynn, Nuclear cross-relaxation induced by specimen rotation, *Phys. Lett.* **4,** 99–100 (1963).
11. D. P. Raleigh, M. H. Levitt, and R. G. Griffin, Rotational resonance in solid state NMR, *Chem. Phys. Lett.* **146,** 71–76 (1988).
12. W. E. J. R. Maas, and W. S. Veeman, Natural abundance ^{13}C spin diffusion enhanced by magic-angle spinning, *Chem. Phys. Lett.* **149,** 170–174 (1988).
13. M. G. Colombo, B. H. Meier, and R. R. Ernst, Rotor-driven spin diffusion in natural-abundance ^{13}C spin system, *Chem. Phys. Lett.* **146,** 189–196 (1988).
14. M. H. Levitt, D. P. Raleigh, F. Creuzet, and R. G. Griffin, Theory and simulations of homonuclear spin pairs systems in rotating solids, *J. Chem. Phys.* **92,** 6347–6364 (1990).
15. A. Kubo and C. A. McDowell, ^{31}P spectral spin diffusion in crystalline solids, *J. Chem. Phys.* **89,** 63–70 (1988).
16. J. Baum, M. Munowitz, A. N. Garroway, and A. Pines, Multiple-quantum dynamics in solid state NMR, *J. Chem. Phys.* **83,** 2015–2025 (1985).
17. B. H. Meier and W. L. Earl, Excitation of multiple quantum transitions under magic angle spinning conditions: Adamantane, *J. Chem. Phys.* **85,** 4905–4911 (1986).
18. G. Wingefeld and R. Hoppe, Zur konstitution von $Ba_2WO_3F_4$ und $Ba_2MoO_3F_4$, *Z. Anorg. Allg. Chem.* **518,** 149–160 (1984).
19. V. R. Domesle and R. Hoppe, Zur kenntnis von $Ba_2WO_3F_4$ und weiterer oxidfluoride mit wolfram and molybdän, *Z. Anorg. Allg. Chem.* **492,** 63–68 (1982).
20. C. C. Torardi and L. H. Brixner, Structure and luminescence of $Ba_2WO_3F_4$, *Mat. Res. Bull.* **20,** 137–145 (1985).
21. A. Abragam, "Principles of Nuclear Magnetism," Clarendon Press, Oxford (1961).
22. P. Robyr, B. H. Meier, and R. R. Ernst, Radio-frequency-driven nuclear spin diffusion in solids, *Chem. Phys. Lett.* **162,** 417–423 (1989).
23. A. E. Bennett, J. H. Ok, R. G. Griffin, and S. Vega, Chemical shift correlation spectroscopy in rotating solids: Radio frequency-driven dipolar recoupling and longitudinal exchange, *J. Chem. Phys.* **96,** 8624–8627 (1992).
24. Y. K. Lee, N. D. Kurur, M. Helmle, O. G. Johannessen, N. C. Nielsen, and M. H. Levitt, Efficient dipolar recoupling in the NMR of rotating solids. A sevenfold symmetric radiofrequency pulse sequence, *Chem. Phys. Lett.* **242,** 304–309 (1995).
25. M. Feike, D. E. Demco, R. Graf, J. Gottwald, S. Hafner, and H. W. Spiess, Broadband multiple-quantum NMR spectroscopy, *J. Magn. Reson.* **122,** 214–221 (1996).
26. H. Geen, J. Gottwald, R. Graf, I. Schnell, H. W. Spiess, and J. J. Titman, Elucidation of dipolar coupling networks under magic-angle spinning, *J. Magn. Reson.* **125,** 224–227 (1997).